User Guide v2.1

CS2SMOS: Weekly Arctic Sea-Ice Thickness Data Record

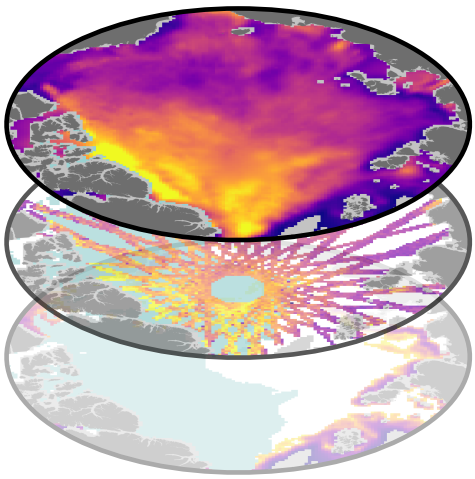

Authors

Robert Ricker[1,2]
Stefan Hendricks[1]
Lars Kaleschke[3]
Xiangshan Tian-Kunze[3]

[1]Alfred Wegener Institute, Helmholtz Centre for Polar and Marine Research, Bremerhaven
[2]Univ. Brest, CNRS, IRD, Ifremer, Laboratoire d'OcÈanographie Physique et Spatiale (LOPS), IUEM, 29280, Brest, France
[3]University of Hamburg, Germany

Alfred-Wegener-Institut Helmholtz-Zentrum für Polar- und Meeresforschung
August 2016

Change Log

Document Rev.	Product Rev.	Date	Changes
1.0	1.0	02.12.2015	Initial version
2.0	1.1	01.06.2016	Major algorithm changes:
			New background field estimate
			New background field estimate
			New correlation length scale estimate
			Applying OSI SAF ice type product to exclude SMOS data over multiyear ice
			Documentation changes
2.1	1.1	23.08.2016	Minor changes in the document

Important Note

This service is not an operational data service. Updates on weekly ice thickness fields will happen irregularly and revisions of the entire data time series might occur at any time. This product shall be a tool for the scientific community to enable further development of sea ice thickness retrieval algorithms and not be used in the sense of a fully calibrated and validated data product. It is our aim however, to implement progress in algorithm development in new revisions. We encourage users to give feedback (info@meereisportal.de) for further improvements of the CryoSat-2/SMOS data fusion product.

1 Introduction

1.1 Purpose of this document

The purpose of this document is to describe the data fusion and the objective mapping algorithm base of the CS2SMOS intermediate climate data record (ICDR), which has been developed within the framework of the SMOS+Sea ice project, funded by the European Space Agency. This document provides a description of the algorithm applied to merge the individual CryoSat-2 (CS2) and Soil Moisture and Ocean Salinity (SMOS) sea-ice thickness products, as well as output data format specifications. Furthermore, characteristics of the data fusion product are illustrated in order to inform about the differences to the individual products.

1.2 Motivation and Scope of the CS2-SMOS Data Fusion

The SMOS mission provides L-band observations and the ice thickness-dependency of brightness temperature enables to estimate the sea-ice thickness for thin ice regimes, in particular during the freeze-up (Kaleschke et al., 2012). On the other hand, CS2 uses radar altimetry to measure the height of the ice surface above the water level, which can be converted into sea-ice thickness assuming hydrostatic equilibrium. In contrast to SMOS, The CS2 mission was primary designed to measure the thickness of the perennial ice cover and lacks the sensitivity for thin ice regimes (Wingham et al., 2006).

The complementary nature of the relative uncertainties of CS2 and SMOS ice thickness retrievals has been shown by Kaleschke et al. (2015). Figure 1 illustrates uncertainty maps and the relative uncertainties of CS2 and SMOS monthly means from March 2016. The SMOS ice thickness uncertainty is provided as a lower and upper estimate and currently under revision. While the SMOS relative uncertainties are lowest for very thin ice, CS2 relative thickness uncertainties are smaller over thick ice and rise asymptotic towards thickness values < 1 m, which is due to the different methodical approach. We acknowledge that the CS2 uncertainties represent statistical uncertainties only. Systematic errors as due to the usage of a snow climatology as well as snow-volume scattering may alter the uncertainty estimate (Ricker et al., 2014, 2015).

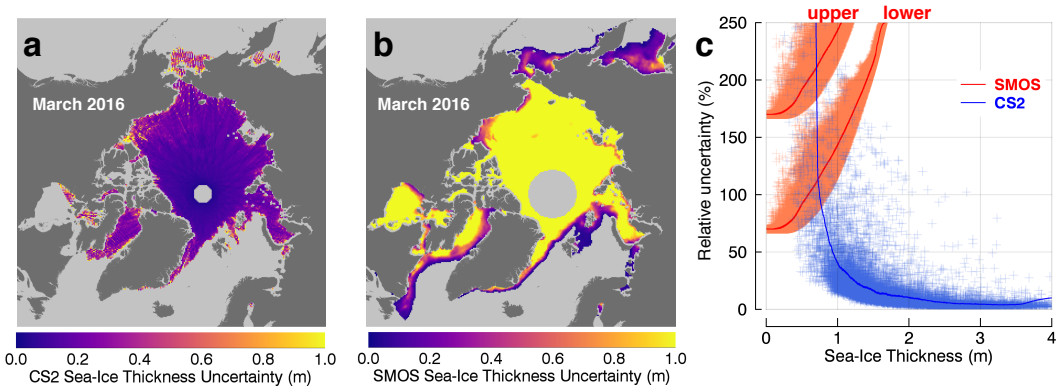

Figure 1: Monthly sea-ice thickness uncertainty maps of the CryoSat-2 (a) and SMOS (b) retrieval for March 2016, where SMOS uncertainties are represented by the lower estimate. c) Relative uncertainties from March 2016.

However, also the spatial coverage is of complementary nature due to the different orbital inclinations. Figure 2 shows weekly means of CS2 and SMOS during the freezing season 2015/16. While valid SMOS ice thickness estimates can be found mostly in the marginal ice zones, the CS2 ice thickness retrieval covers major parts of the Arctic multiyear ice (MYI). Figure 3 illustrates the number of valid grid cells of the weekly means as shown in Figure 2. The number of grid cells, which share SMOS and CS2 estimates, is significantly lower than of grid cells that contain thickness estimates from one sensor exclusively.

Hence, a data fusion of CS2 and SMOS sea-ice thickness retrievals has the capability to complete Arctic sea-ice thickness distributions. Therefore, we aim to develop a method to merge both data sets on a suitable spatial and temporal scale.

1.3 Further Information

Additional information of the CryoSat-2 and SMOS missions as well as other ESA data products can be found on the following websites:

- ESA - Living Planet Program- CryoSat-2
- ESA - Living Planet Program- SMOS

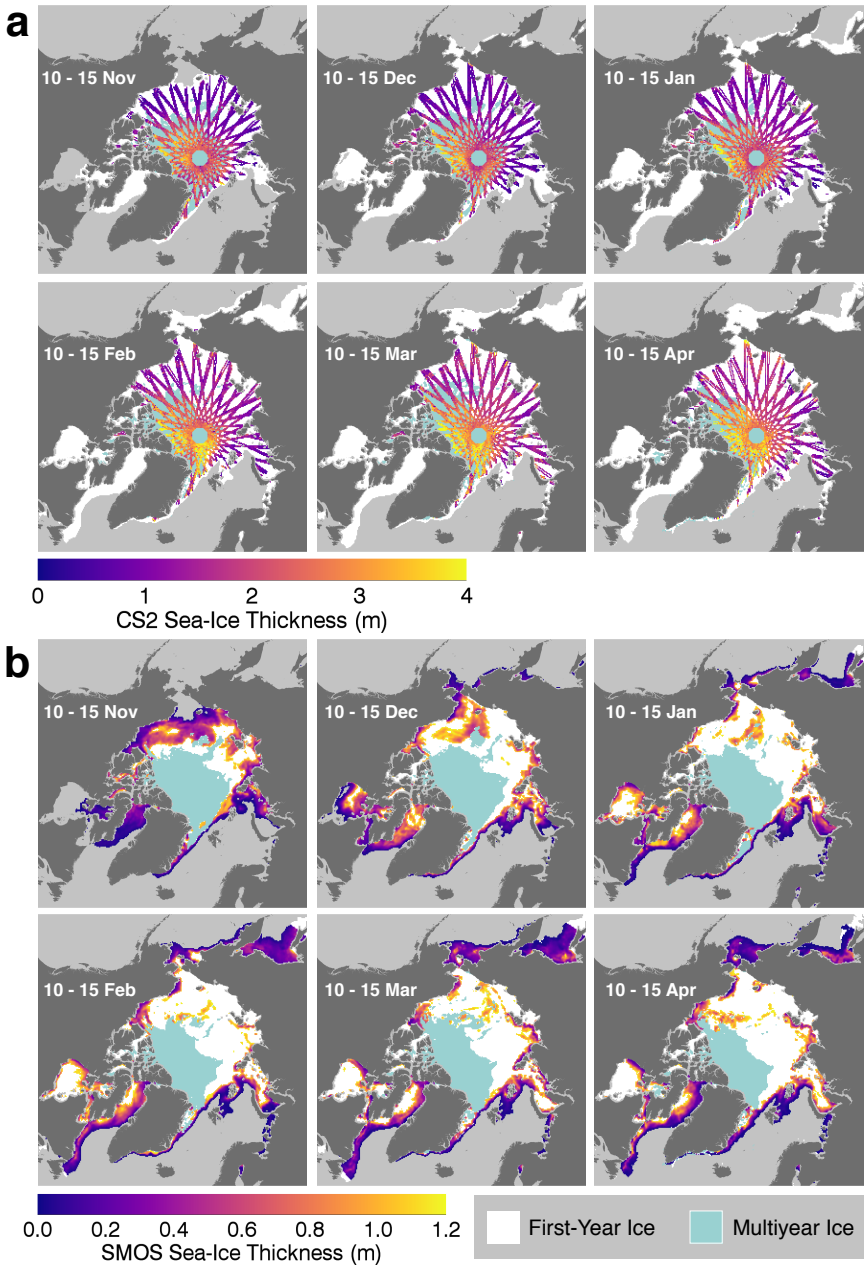

Figure 2: Weekly input data grids for the freezing season November-April 2015/16. a) Weekly CryoSat-2 retrieval as used for the objective mapping. b) Weekly means of daily SMOS ice thickness retrievals, cropped by a 3 m maximum SMOS thickness uncertainty filter. The background indicates first-year and multiyear ice coverage. Note the complementary coverage in a) and b).

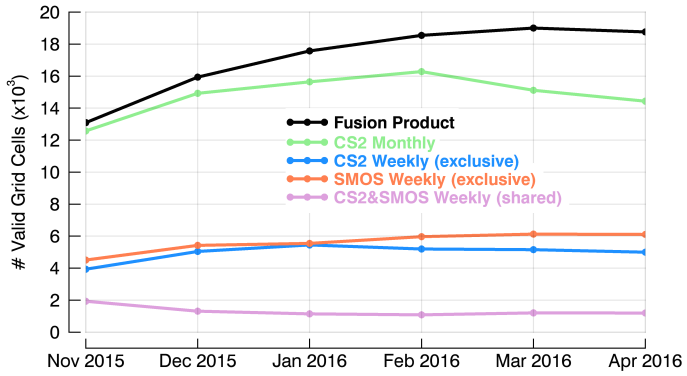

Figure 3: Spatial coverage in number of valid 25 km grid cells. Here, the term *valid* means that the grid cell contains a valid thickness estimate. The fusion product and other weekly retrievals are represented by weeks illustrated in Figure 2.

2 Methods

We use an optimal interpolation scheme (OI) similar to Böhme and Send (2005); Boehme et al. (2008); McIntosh (1990) that enables the merging of datasets from divers sources on a predefined, so-called analysis grid. The data are weighted differently based on known uncertainties of the individual products and modeled spatial covariances. OI minimizes the total error of observations and provides ideal weighting for the observations at each grid cell.

In this section we present the processing methods, on which the here presented objective mapping is based on. Figure 4 shows the processing scheme which will be described in more detail in the following. The OI scheme is used to get an objective estimate of values at unobserved locations. The basic equation is:

$$\mathrm{T_a} = \mathrm{T_b} + \mathrm{K}[\mathrm{T_o} - \mathrm{H}(\mathrm{T_b})], \tag{1}$$

where the vector T_a is the analysis field that represents the merged CS2-SMOS ice thickness retrieval which we aim for. T_b is the background field vector and T_o the vector that contains all observations (SMOS and CS2). As observations we define already gridded thickness estimates, based on weekly averages as shown in Figure 2. We do this to reduce statistical uncertainties and to provide rather equally distributed observations, which improves the performance of the OI. Furthermore, it is reasonable

Table 1: Properties of input and output data grids, which are used to obtain the data fusion product.

Product	Source	Frequency	Spatial coverage	Grid/resolution
SMOS Ice Thickness	icdc.zmaw.de/daten	Daily	Entire Arctic	Polarstereo 12.5 km
CS2 Ice Thickness	data.seaiceportal.de	Weekly	Incomplete	EASE2 25 km
Ice Concentration	osisaf.met.no/p/ice/	Daily	Entire Arctic	Polarstereo 10 km
Ice Type	osisaf.met.no/p/ice/	Daily	Entire Arctic	Polarstereo 10 km
Fusion Product	data.seaiceportal.de	Weekly	Entire Arctic	EASE2 25 km

to reduce the number of observations, otherwise computing can become expensive. Moreover, we assume that the observations are static, which is a simplification, because the satellite thickness estimates are temporally dependent due to ice dynamics and ice drift. Therefore, we neglect any temporal correlations. H is an operator that transforms the background field into the observation space. To be more specific, this is realized by an inverse distance interpolation method. We aim to retrieve weekly analysis fields, based on calendar weeks that reach from Monday to Sunday. Melting does not allow to retrieve summer sea-ice thickness estimates neither from CS2 nor SMOS. Hence, the fusion Product is limited to the period from October/November to April.

2.1 Data Sources

As input ice thickness data we use the AWI CS2 product (processor version 1.2) (Ricker et al., 2014; Hendricks et al., 2016) and the SMOS sea-ice thickness retrieval from the University of Hamburg (processor version 3.0) (Tian-Kunze et al., 2014; Kaleschke et al., 2016). As auxiliary data we use ice concentration and ice type provided by the Ocean and Sea Ice Satellite Application Facility (OSI SAF). Table 1 summarizes the different input grids and their spatial resolution.

2.2 The Background Field

The CS2 weekly products leave gaps due to the incomplete orbital coverage (Figure 2a). Therefore, we compute an averaged composite of weekly retrievals, ranging from 2 weeks behind to two weeks ahead, to get a nearly complete coverage for the Arctic (Figure 5) at a certain target week.

The daily SMOS retrievals are averaged weekly and then re-gridded on an EASE2 25 km grid to be in line with the CS2 retrieval. Here, we only allow SMOS thickness values with a corresponding upper uncertainty < 3m which corresponds to a maximum theoretical thickness of 1.2 m. Furthermore we expect strong biases for the SMOS ice thickness in thicker MYI regimes. Therefore we apply the OSI SAF ice type product (Eastwood, 2012) and discard any SMOS grid cells that are indicated as MYI. The weekly composites of CS2 and SMOS are shown in Figure 2.

The initial background field is then represented by a weighted average:

$$\overline{\mathrm{T}} = \frac{\mathrm{T_{cs2}}/\sigma_{cs2}^2 + \mathrm{T_{smos}}/\sigma_{smos}^2}{1/\sigma_{cs2}^2 + 1/\sigma_{smos}^2}. \tag{2}$$

T is the ice thickness and σ the statistical uncertainty of the individual products. Since we use CS2 and SMOS retrievals for the background field beyond the target week and because the SMOS composite contains artifacts of very thin ice (< 10 cm) in coastal regions, we additionally use an ice concentration mask, likewise a weekly mean of daily retrievals from the OSI SAF ice concentration product (Eastwood, 2012) to guarantee the ice coverage during the target week. Here, we use a threshold of 15 % and only grid cells which exceeds this value will be considered as ice covered, which corresponds to the ice extent products provided by OSI SAF and the National Snow and Ice Data Center (NSIDC). Gaps in the weighted average, derived from Eq. 2 are interpolated by a nearest neighbor scheme. In order to reduce noise, the background field is low-pass filtered before it is used for objective mapping (Figure 5b).

2.3 The Optimal Interpolation Algorithm

The weight matrix K, which is needed to calculate T_a, is retrieved by the background error covariance matrix B in the observation space, multiplied by the inverted total error covariance matrix:

$$\mathrm{K} = \mathrm{BH^T}(\mathrm{R} + \mathrm{HBH^T})^{-1}, \tag{3}$$

where R is the error covariance matrix of the observations. In order to reduce computation expense we do several assumptions:

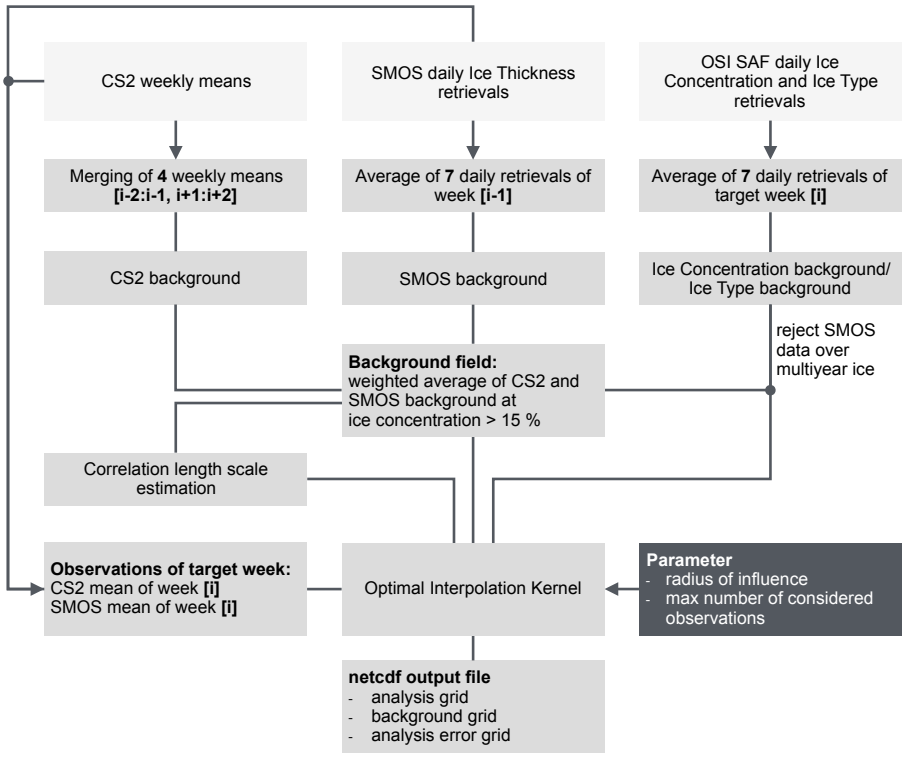

Figure 4: Objective mapping processing scheme. [i] represents the target week. The cycle is repeated for each week.

1. We neglect correlations of observation errors which means that R is a matrix with non-zero elements only on the diagonal. These variances are represented by the SMOS and CS2 product uncertainties.

2. We assume that the influence of observations that are located far away from the analysis grid point can be neglected. Therefore, instead of computing the entire covariance matrix, we only consider observations within a radius of influence. This radius is set to 250 km to gather just enough observations in regions which large gaps, for example over thick MYI, between two CS2 orbits where valid SMOS observations do not exist.

3. To further reduce computation expense we limit the number of matched observations to 120, meaning that in the case of more matches, only the 120 closest observations are considered.

4. We generally assume that all observations are unbiased, which might be not true

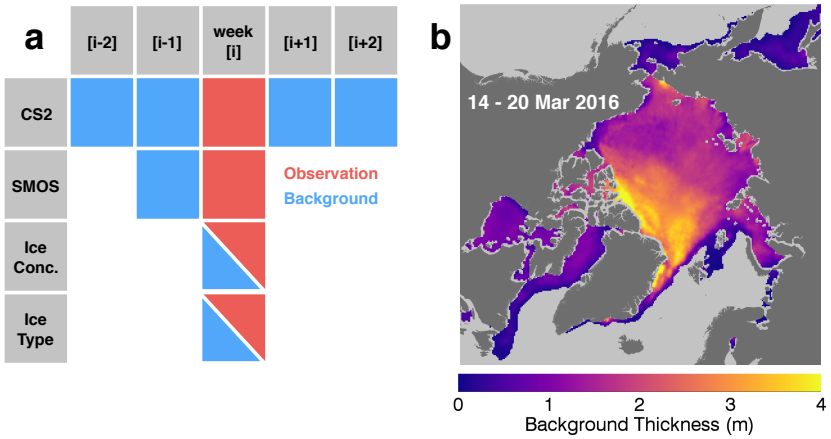

Figure 5: a) The scheme illustrates the usage of weekly input grids for the background field and the observation field. [i] represents the target week. b) Interpolated and low-pass filtered background field as it is used for the objective mapping.

in any case (Ricker et al., 2014).

Finally, we use a Markov form as a function of the distance to estimate $\mathrm{BH^T}$ and $\mathrm{HBH^T}$:

$$\begin{aligned} \mathrm{BH^T} &= (1 + (\mathrm{d}(\mathrm{x_{o_i}}, \mathrm{x_{a_i}})/\mathrm{cls}))\exp(-\mathrm{d}(\mathrm{x_{o_i}}, \mathrm{x_{a_i}})/\mathrm{cls}) \\ \mathrm{HBH^T} &= (1 + (\mathrm{d}(\mathrm{x_{o_i}}, \mathrm{x_{o_j}})/\mathrm{cls}))\exp(-\mathrm{d}(\mathrm{x_{o_i}}, \mathrm{x_{o_j}})/\mathrm{cls}) \end{aligned} \tag{4}$$

with the Euclidian distance function:

$$\mathrm{d}(\mathrm{x}, \mathrm{y}) = \|\mathrm{x} - \mathrm{y}\|_2 \tag{5}$$

Here, $\mathrm{x_{o_i}}$ and $\mathrm{x_{a_i}}$ represent locations of the observations and analysis grid points. The Markov function serves to model the spatial correlation function, which is then scaled with the variances of the observation ensemble. Thus, the impact of a data point decreases with increasing distance. The calculation of cls is described in section 2.4.

After computing $\mathrm{BH^T}$ and $\mathrm{HBH^T}$, yielding K, we retrieve the second term of Eq. 1, which is called innovation. This iterative procedure is done for every analysis grid point, leading us to the complete analysis grid T_a.

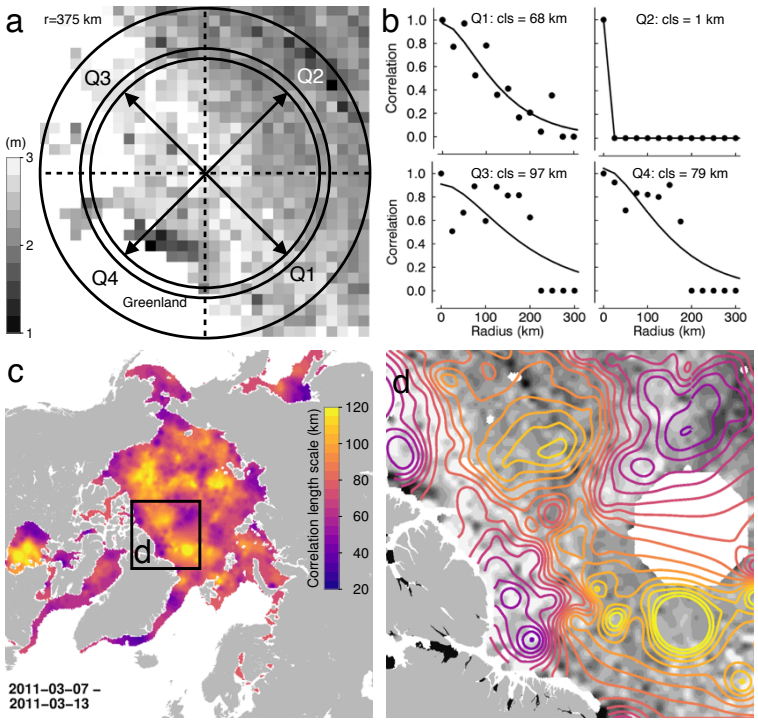

Figure 6: Estimation of the correlation length scale (cls) for a single grid cell (a): adjacent ice thickness grid cells within a radius of 375 km are binned into annuli of distance and 4 quadrants. (b) Binned thickness estimates are used to calculate the structure function of each quadrant. The cls is estimated by fitting an exponential function. c) Map of estimated correlation length scales for the 1st week of March 2011. d) The enlarged area shows contoured length scales on top of gray-scaled background thickness with the color scale as in a).

2.4 Correlation Length Scale Estimation

The correlation length scale cls controls how strong the exponential function decreases with distance. Since we work on a 25 km grid, we will only consider large scale correlations. Ideally, our correlation length scale estimate is large in the center of a certain ice type regime with similar ice thickness (i.e. first year ice). On the other hand, we expect a low cls value at locations with a steep thickness gradient. In order to estimate the spatial distribution of cls, we consider the unfiltered background field T_b. In the following we define a structure function ϵ^2, which is related to the normalized auto correlation function

R(d,Q) as follows (Böhme and Send, 2005):

$$\epsilon^2(\mathrm{d},\mathrm{Q}) = \overline{(\mathrm{T}'_0 - \mathrm{T}'_{\mathrm{Q,d}})^2} = 2\overline{\sigma^2_{T'}} - 2\overline{\sigma^2_{T'}}\mathrm{R}(\mathrm{d},\mathrm{Q})$$
$$\mathrm{R}(\mathrm{d},\mathrm{Q}) = 1 - \frac{\epsilon^2(\mathrm{d},\mathrm{Q})}{2\overline{\sigma^2_{T'}}} \quad (6)$$

We define quadrants Q to accommodate the anisotropy of the spatial ice thickness distribution (Figure 6a). $\epsilon^2(d,Q)$ represents the square differences between ice thickness of the grid cell and the ice thickness of the grid cells of binned 25 km distances d in a quadrant Q. $\mathrm{T}'_{\mathrm{Q,d}}$ is the unfiltered background thickness, binned according to d and Q. $\overline{\sigma^2_{T'}}$ are the corresponding mean variances of a certain quadrant. With Eq. 6 we can then obtain the auto correlation function R(d,Q), which is computed up to radius of 750 km (30 bins). In the next step, we fit a Markov function to R(d,Q) and therefore get an estimate for cls. Figure 6 shows how cls is derived. Figure 6a reveals the annuli of distance and the 4 Quadrants. Figure 6b shows the calculated auto correlation function R(d,Q) and the fitted Markov function. Note the strong decrease of $\epsilon^2(d,Q)$ in Q2, which is because T_0 belongs to a thicker ice regime, while the regime in Q3 is consistently thinner. Therefore $\epsilon^2(\mathrm{d},\mathrm{Q})$ rises, while $\overline{\sigma^2_{T'}}$ is small. This leads to a strong decrease of R(d,Q) with the distance. R(d,Q) can also become negative if ϵ^2 (d,Q)/2 $\overline{\sigma^2_{T'}}$ gets $>$1. In order to enhance the fitting performance, we set R(d,Q) = 0 if R(d,Q) < 0. Furthermore cls is set to NaN (not-a-number) if the computation failed. Finally, we take the mean of the cls values from the 4 quadrants. In order to remove outliers and noise, the derived cls grid is low-pass filtered with a smoothing radius of 25 km. Invalid grid cells are interpolated by a nearest neighbor scheme afterwards. Figure 6c shows the spatial correlation length scales cls for 7-13 March 2011. The enlarged area in Figure 6d shows how the cls decreases in areas with high sea ice thickness gradients.

2.5 The Analysis Error Field

The analysis error covariances are derived by:

$$\sigma^2_{T_a} = (\mathrm{I} - \mathrm{KH})\mathrm{B} \quad (7)$$

Since we consider variances exclusively, we only calculate the diagonal elements of $\sigma^2_{T_a}$. Figure 7 shows the data fusion product and furthermore the innovation field and

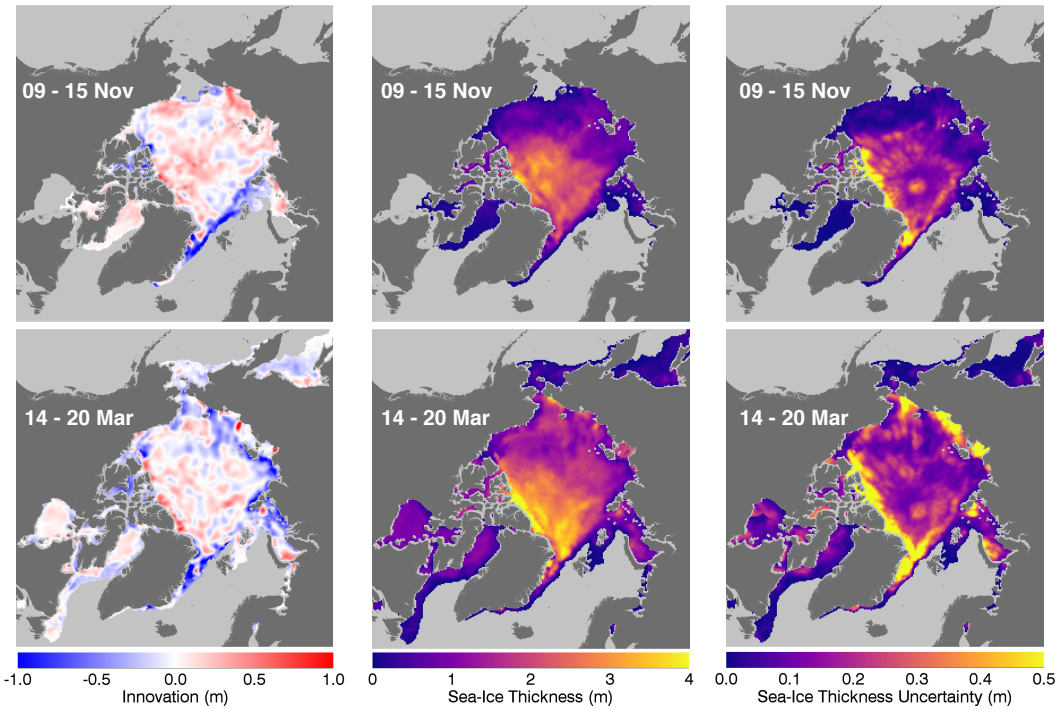

Figure 7: Output grids from the objective mapping processing for weeks in November 2015 and March 2016: The innovation (left column) is the difference between background and the fusion product ice thickness (center column). The sea-ice thickness uncertainty of the objective mapping product is derived from the relative analysis error, scaled with the observation variances (right column).

the analysis error, which is the root of the error variance. The analysis error is a relative quantity with values between 0 and 1, which is scaled with observation variances in this figure. It increases where the weekly CS2 retrieval leaves gaps and where valid SMOS observations are not available, for example at the North Pole or over MYI. In this case the analysis heavily depends on the background field, and therefore the error increases.

3 Dynamic Range of the Fusion Product

Figure 8 shows ice thickness distributions of monthly means of CS2 and SMOS ice thickness retrievals and the weekly fusion product during the freezing season 2015/16. It illustrates the different thickness domains of CS2 and SMOS. The CS2 retrieval lacks sensitiv-

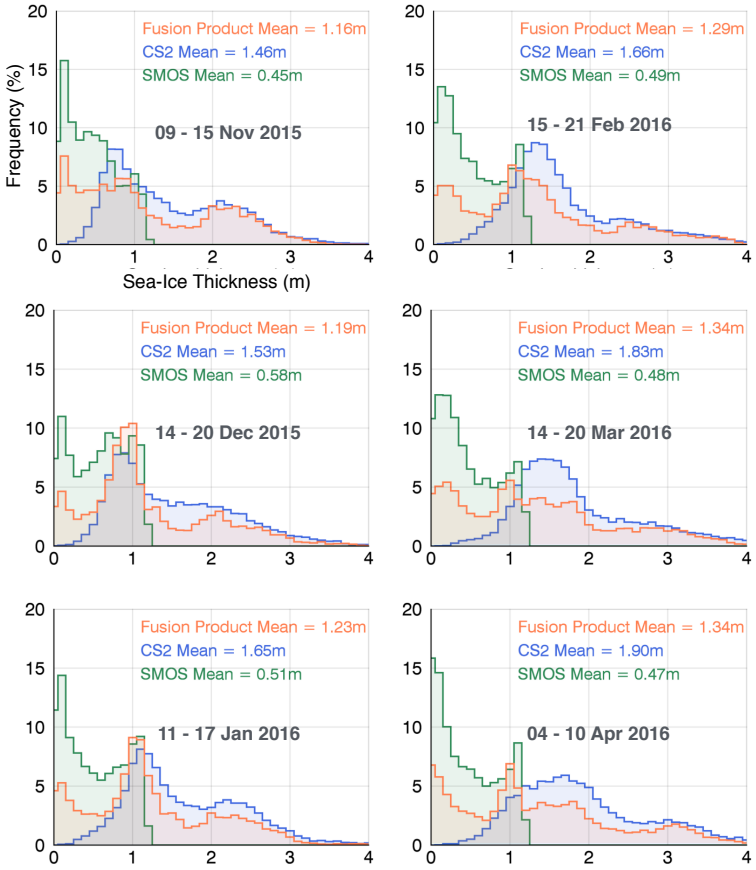

Figure 8: Sea-ice thickness distributions corresponding to Figure 2 during the freezing season 2015/16. The fusion product is represented by one week within each month, while the CryoSat-2 and SMOS retrievals are monthly means.

ity for thin ice (< 0.8 m). This gap can be closed by the SMOS retrieval. Due to the lack of sensitivity over thick ice and the maximum uncertainty filter, the frequency drops steeply at about 1 m. The data fusion product shows its capability to combine both the CS2 and the SMOS ice thickness domains.

4 Data Description

The weekly analysis grids are given in standardized binary data format (Network common data form: NetCDF v3). The variables are given as grid arrays, see therefore Table 2. All grids are projected onto the 25 km EASE2 Grid, which is based on a polar

aspect spherical Lambert azimuthal equal-area projection (Brodzik et al., 2012) (Figure 9).

Table 2: Netcdf file content and description of variables.

Variable	Description	Unit	Type	Dimension
xc	EASE2 grid x coordinates	km	double	720
yc	EASE2 grid y coordinates	km	double	720
longitude	Longitude	deg east	double	720,720
latitude	Latitude	deg north	double	720,720
analysis_thickness	Analysis sea-ice thickness	m	float	720,720
analysis_thickness_err	Relative error of the analysis thickness	arbitrary unit	float	720,720
background_thickness	Sea-ice thickness background field	m	float	720,720
corr_scale	Correlation length scale	m	float	720,720
cs2_thickness	Weekly averaged CryoSat-2 thickness	m	float	720,720
smos_thickness	Weekly averaged SMOS thickness	m	float	720,720
innovation	Difference background/analysis field	m	float	720,720
ice_concentration	Sea-ice concentration (from OSI SAF)	%	float	720,720
ice_type	Sea-ice type (from OSI SAF)	binary	float	720,720

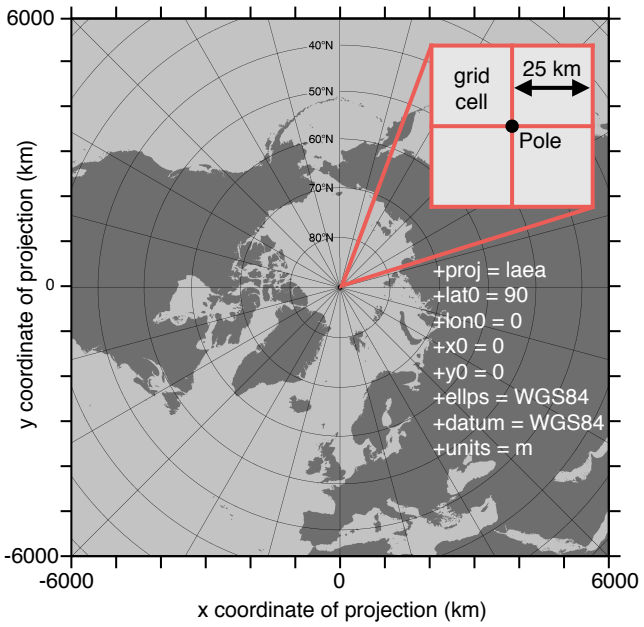

Figure 9: Specifications of the EASE2 25 km grid, which is used for the data fusion product.

Acknowledgements

This work was funded by the European Space Agency (contracts 4000101476/10/NL/CT and 4000112022/14/I-AM) and the Deutsche Forschungsgemeintschaft (DFG EXC177).

References

Boehme, L., Meredith, M. P., Thorpe, S. E., Biuw, M., and Fedak, M.: Antarctic Circumpolar Current frontal system in the South Atlantic: Monitoring using merged Argo and animal-borne sensor data, Journal of Geophysical Research: Oceans, 113, doi: 10.1029/2007JC004647, URL http://dx.doi.org/10.1029/2007JC004647, c09012, 2008.

Böhme, L. and Send, U.: Objective analyses of hydrographic data for referencing profiling float salinities in highly variable environments, Deep Sea Research Part II: Topical Studies in Oceanography, 52, 651–664, 2005.

Brodzik, M. J., Billingsley, B., Haran, T., Raup, B., and Savoie, M. H.: EASE-Grid 2.0: Incremental but Significant Improvements for Earth-Gridded Data Sets, ISPRS International Journal of Geo-Information, 1, 32–45, doi:10.3390/ijgi1010032, URL http://www.mdpi.com/2220-9964/1/1/32, 2012.

Eastwood, S.: OSI SAF Sea Ice Product Manual, v3.8 edn., URL http://osisaf.met.no, 2012.

Hendricks, S., Ricker, R., and Helm, V.: User Guide - AWI CryoSat-2 Sea Ice Thickness Data Product (v1.2), 2016.

Kaleschke, L., Tian-Kunze, X., Maaß, N., Mäkynen, M., and Drusch, M.: Sea ice thickness retrieval from SMOS brightness temperatures during the Arctic freeze-up period, Geophysical Research Letters, 39, 2012.

Kaleschke, L., Tian-Kunze, X., Maas, N., Ricker, R., Hendricks, S., and Drusch, M.: Improved retrieval of sea ice thickness from SMOS and CryoSat-2, in: Geoscience and Remote Sensing Symposium (IGARSS), 2015 IEEE International, pp. 5232–5235, IEEE, 2015.

Kaleschke, L., Tian-Kunze, X., Maaß, N., Beitsch, A., Wernecke, A., Miernecki, M., Müller, G., Fock, B. H., Gierisch, A. M., Schlünzen, K. H., Pohlmann, T., Dobrynin, M., Hendricks, S., Asseng, J., Gerdes, R., Jochmann, P., Reimer, N., Holfort, J., Melsheimer, C., Heygster, G., Spreen, G., Gerland, S., King, J., Skou, N., Søbjærg, S. S., Haas, C., Richter, F., and Casal, T.: {SMOS} sea ice product: Operational application and validation in the Barents Sea marginal ice zone, Remote Sensing of Environment, 180, 264 – 273, doi:http://dx.doi.org/10.1016/j.rse.2016.03.009, URL http://www.sciencedirect.com/science/article/pii/S003442571630102X, special Issue: ESA's Soil Moisture and Ocean Salinity Mission - Achievements and Applications, 2016.

McIntosh, P. C.: Oceanographic data interpolation: Objective analysis and splines, Journal of Geophysical Research: Oceans (1978–2012), 95, 13 529–13 541, 1990.

Ricker, R., Hendricks, S., Helm, V., Skourup, H., and Davidson, M.: Sensitivity of CryoSat-2 Arctic sea-ice freeboard and thickness on radar-waveform interpretation, The Cryosphere, 8, 1607–1622, doi:10.5194/tc-8-1607-2014, URL http://www.the-cryosphere.net/8/1607/2014/, 2014.

Ricker, R., Hendricks, S., Perovich, D. K., Helm, V., and Gerdes, R.: Impact of snow accumulation on CryoSat-2 range retrievals over Arctic sea ice: An observational approach with buoy data, Geophysical Research Letters, 42, 4447–4455, doi:10.1002/2015GL064081, URL http://dx.doi.org/10.1002/2015GL064081, 2015GL064081, 2015.

Tian-Kunze, X., Kaleschke, L., Maaß, N., Mäkynen, M., Serra, N., Drusch, M., and Krumpen, T.: SMOS-derived thin sea ice thickness: algorithm baseline, product specifications and initial verification, The Cryosphere, 8, 997–1018, doi:10.5194/tc-8-997-2014, URL http://www.the-cryosphere.net/8/997/2014/, 2014.

Wingham, D., Francis, C., Baker, S., Bouzinac, C., Brockley, D., Cullen, R., de Chateau-Thierry, P., Laxon, S., Mallow, U., Mavrocordatos, C., Phalippou, L., Ratier, G., Rey, L., Rostan, F., Viau, P., and Wallis, D.: CryoSat: A mission to determine the fluctuations in Earth's land and marine ice fields, Advances in Space Research, 37, 841 – 871, doi:10.1016/j.asr.2005.07.027, 2006.